Chemical Engineering Journal 272 (2015) 108–118

Contents lists available at ScienceDirect

Chemical Engineering Journal

journal homepage: www.elsevier.com/locate/cej

Glycerol steam reforming over layered double hydroxide-supported Pt catalysts

Simone M. de Rezende [a,1], Carlos A. Franchini [a], Maria Laura Dieuzeide [b], Andréa M. Duarte de Farias [a], Norma Amadeo [b,*], Marco A. Fraga [a,*]

[a] Instituto Nacional de Tecnologia, Laboratório de Catálise, Av. Venezuela, 82/518, 20081-312 Rio de Janeiro, RJ, Brazil
[b] ITHES (CONICET – Universidad de Buenos Aires), Pabellón Industrias, Ciudad Universitaria, 1428 Buenos Aires, Argentina

HIGHLIGHTS

- Glycerol reforming on catalysts obtained from MgAl layered double hydroxides.
- Weak to moderate basic sites render catalysts more selective to hydrogen.
- More stable carbon deposits play major role in catalyst deactivation.
- Highly dispersed metal sites are important for *in situ* catalyst surface cleanness.

GRAPHICAL ABSTRACT

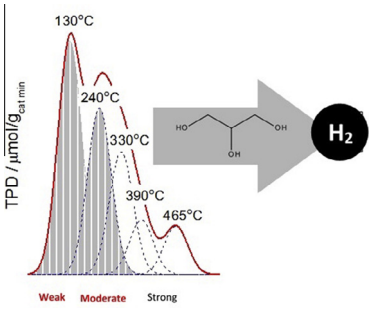

ARTICLE INFO

Article history:
Received 12 December 2014
Received in revised form 4 March 2015
Accepted 7 March 2015
Available online 16 March 2015

Keywords:
Glycerol
Steam reforming
Hydrogen production
Deactivation
LDH
Carbon deposition

ABSTRACT

Layered double hydroxides containing Mg and Al (Mg/Al ratios of 3 and 5) were used as support for Pt-based catalysts for glycerol steam reforming. Additionally, catalysts supported on the parent MgAl mixed oxides were also evaluated. Fresh catalyst samples were characterized by XRD, BET, TPD-CO_2 and XRF whilst the spent catalysts were examined by TEM and TPO/TGA-MS. All catalysts revealed to be active, leading to a hydrogen-rich gas stream but with distinct resistance to deactivation. The catalyst synthesized directly from the layered double hydroxide precursors with Mg/Al ratio of 3 was shown to be more effective since global and gas conversion are similar, varying within 60–25%. Major incidence of weak to moderate basic surface centers rendered catalysts more selective, reaching up to 68% selectivity to hydrogen. However, they were not enough to suppress deactivation. It was found that the formation of more stable carbon deposits play a key role on deactivation and only a minor contribution from the carbonaceous material formed from the intermediate organic liquid compounds was proposed. Highly dispersed metal centers were suggested to be important for *in situ* catalyst surface cleanness.

1. Introduction

Hydrogen can be utilized in clean power generation through the employment of devices known as fuel cells. Different routes are known for producing hydrogen, mostly by applying thermochemical reactions based on a number of fossil and renewable feedstocks such as methane, ethanol, bio-oil, ethylene glycol, glycerol, etc. Time and effort have been spent on studying hydrogen production motivated by the promise of energy offer associated with very low levels of pollutant emissions. Additionally, the hydrogen technology platform can be enhanced by preferentially choosing renewable resources as main raw materials. They can certainly create benefits but also bring some technical challenges. In fact, in spite

* Corresponding authors.
E-mail addresses: norma@di.fcen.uba.ar (N. Amadeo), marco.fraga@int.gov.br (M.A. Fraga).
[1] Present address: SENAI CETIQT, Unidade Riachuelo, R. Magalhães Castro, 174, Riachuelo, 20961-020 Rio de Janeiro, RJ, Brazil.

http://dx.doi.org/10.1016/j.cej.2015.03.033
1385-8947/

of the sustainability assessment brought about by this matter, economic competitiveness must also be considered. In this context, the increasing availability of glycerol as a co-product of biodiesel production makes it attractive to address these issues.

Glycerol is a particularly interesting biomass-derived compound in todaýs global scenario given the ever-growing application of biodiesel as fuel component worldwide. This is additionally motivated by the vast accessibility to oleaginous seeds in many countries, such as Brazil. The thermochemical transformation of glycerol to hydrogen has been assessed by pyrolysis and different types of reforming reactions. Amongst them aqueous phase (APR) [1–4], dry [5] and steam reforming reactions (SR) [6–11] are being consistently studied. Those are catalyzed reactions conducted over metal based formulations. Usually the catalysts are composed by Ni, Co, Ru, Rh, Ir or Pt [1–11], all having the ability to promote the cleavage of C–C, O–H and C–H bonds.

Based on its low cost, availability and good performance, Ni is the most cited metal appearing in the dedicated literature. However, as already reported in previous investigations regarding alcohol reforming reactions [3,6,12–15], noble metals also present potential performance in glycerol reforming [6,15–18]. These metals are worth studying because they are active and stable at low temperature. As a consequence, they are good candidates to reach some crucial goals in glycerol reforming. Metallic or bimetallic catalysts having platinum as one of the components have showed good performance at temperatures below 350 °C [15]. In a straightforward comparison between Ni and Pt, Pompeo et al. [19] attested that Pt catalysts are more active and much more stable than Ni catalysts. Complete glycerol conversion to gas was achieved over Pt based catalyst, producing a gaseous stream with 70% of hydrogen. Furthermore no deactivation was observed during 40 h on stream. Conversely, strong deactivation caused by carbon deposits with polymeric or amorphous structure was formed on the non-noble metal catalyst [19].

Considering the problem of deactivation, such formation of carbonaceous deposits is indeed the most crucial issue regarding reforming processes for energy generation. As for glycerol reforming, its genesis has been frequently claimed to be related to parallel reactions such as dehydration, dehydrogenation and condensation. These side reactions would lead to the formation of a wide range of intermediate organic compounds [7]. This phenomenon can be favored or avoided by adjusting the reaction conditions [20] or by the nature of the catalyst [3], tuning its surface properties. Indeed, some authors have claimed that the amount of coke increases with the density of strong acid sites [21]. A speculation model of coke formation has been proposed elsewhere [22]. Basically, it relies on the formation of adsorbed species as carbon precursors from glycerol side reactions that would transform into coke on the active sites.

In view of the possible glycerol reforming processes, SR reaction (Eq. (1)) is an attractive route since it can be carried out at atmospheric pressure. On the other hand, it is thermodynamically favored under high temperature conditions as it is an endothermic reaction (ΔH = +123 kJ/mol). In fact, glycerol SR is a quite complex process, resulting from the combination of the two distinct reactions: glycerol decomposition (Eq. (2)) and water gas-shift reaction (Eq. (3)). Methanation (Eq. (4)) is also one of the main reactions that may occur concomitantly with the others, causing a significant loss of hydrogen.

$$C_3H_8O_3 + 3H_2O \rightarrow 3CO_2 + 7H_2 \quad (1)$$

$$C_3H_8O_3 \rightarrow 3CO + 4H_2 \quad (2)$$

$$CO + H_2O \leftrightarrow CO_2 + H_2 \quad (3)$$

$$CO + 3H_2 \rightarrow CH_4 + H_2O \quad (4)$$

$$2CO \leftrightarrow CO_2 + C \quad (5)$$

Along with the above-stated reactions, the high temperature demanded for glycerol SR also favors other side reactions. It can provoke the breaking of glycerol molecules into lower weight oxygenates or hydrocarbons, such as ethane and ethylene. Still, because of the presence of small carbon-containing molecules (CH_4, CO), further transformations, such as the Boudouard reaction (Eq. (5)), may take place and lead to coke deposition.

Noticeably, this rather intricate scenario of simultaneous and successive undesired reactions must be avoided by applying adequate operation conditions and by an efficient design of the catalyst. Thus, while planning SR reactions, the set of appropriate conditions to minimize deactivation must be chosen. Indeed it has already been discussed in thermodynamics studies [23]: medium-high temperature (>320 °C), atmospheric pressure and high water:glycerol ratio (>4). As previously mentioned, the catalyst design should be considered as well. It should typically contain a metal responsible for the selective cleavage of C–C bonds. Moreover, the use of elements bearing alkaline properties is encouraged since it is known that carbon deposition can be suppressed on supports with strong Lewis basicity [24,25]. Some authors has achieved successful results by adding an alkaline earth (Ca, Sr) or rare earth oxides (La, Gd, Pr, Nd, Er) to the support [25,26]. It has been argued that the presence of these oxides increases the adsorption of CO_2 on the catalyst surface. As a consequence it would reduce carbon deposition through the Boudouard reaction (Eq. (5)) by shifting the equilibrium toward CO. The addition of Mg has also shown to enhance the stability and H_2 selectivity in hydrocarbon and alcohols reforming [11,27,28]. Nevertheless, this approach is mostly used with Ni and Co based catalysts as they are synthesized from layered double hydroxides (LDH). These lamellar materials are usually taken as precursors to obtain highly dispersed metal nanoparticles [29,30]. Such small metal sites along with basic surface centers provided by Mg are known to decrease the amount of deposited carbon and increase the catalyst resistance to deactivation [31,32]. Those layered structures, however, are scarcely exploited to obtain noble metal catalysts and only a few contributions concerning the use of Pt, Rh and Pd can be found [33,34].

Hydrotalcite-like layered double hydroxides (LDHs) are natural or synthetic materials consisting of positively charged brucite-like ($Mg(OH)_2$) sheets. LDHs have divalent Mg^{2+} and trivalent ions, for example Al^{3+}, octahedrally coordinated by hydroxyl groups. The excess of positive charge in the layers is compensated by anions located in the interlayer space. The materials with a hydrotalcite-based structure have the general formula $\left[M^{2+}_{1-x}M^{3+}_{x}(OH)_2\right]\left[A^{-}_{n}\right]_{x/a}\cdot yH_2O$, where M^{2+} and M^{3+} represent divalent and trivalent cations in the octahedral sites within the hydroxyl layers, x is equal to the ratio of $M^{3+}/(M^{2+}+M^{3+})$ and A is the interlayer anion [29]. One of the most attractive properties of these solids is the possibility of tuning its basic strength. This property arises from the flexible Mg^{2+}/M^{3+} ratio of its structure. Furthermore, LDHs can be used as precursors of mixed oxides that are easily obtained upon calcination, resulting in well dispersed oxide phases.

In this contribution, layered double hydroxides containing Mg and Al and their derived mixed oxides were synthesized. These materials were taken as support for Pt-based catalysts and investigated in glycerol steam reforming. In this approach, the distribution of metal and basic surface sites was tuned by exploiting the 2D and 3D architectures afforded by the lamellar hydroxides and LDH-derived mixed oxides, respectively.

2. Experimental

2.1. Support synthesis

The LDH materials were prepared by typical co-precipitation method [35] at 70 °C, using aqueous solutions of aluminum and magnesium nitrates. The concentration of the solutions was calculated to vary the Mg:Al molar ratio; two sets of samples with Mg:Al = 3 and Mg:Al = 5 were synthesized. A NaOH solution at 1 mol/L was used as precipitation agent and the pH was kept constant at 10.0. Precipitation step was followed by aging the resulting suspension at 70 °C for 16 h. Carbonate contamination was minimized by purging the reaction vessel with N_2 throughout the whole preparation procedure. The precipitates were filtered and extensively washed. They were designated as Mg*x*Al–H, where *x* = 3 or 5 depending on Mg:Al ratio. These layered solids were further calcined at 500 °C for 4 h in a muffle in order to provide the LDH-derived mixed oxides herein designated as Mg*x*Al–O.

2.2. Preparation of the catalysts

1 wt.% Pt catalysts were prepared by incipient wetness impregnation, using an aqueous solution of $Pt(NH_3)_4NO_3$ as metal precursor. The impregnation procedure was carried out using both the hydrated layered supports (Mg*x*Al–H samples) as well as the calcined mixed oxides, Mg*x*Al–O. The impregnated solids were dried overnight and finally calcined at 500 °C for 4 h. The catalysts were named as PtMg*x*Al–H and PtMg*x*Al–O.

2.3. Standard characterization of supports and supported catalysts

X-ray diffraction (XRD) was carried out in a Rigaku Miniflex using Cu Kα radiation (1.540 Å). The diffraction patterns were recorded in the range of 5–80° (2θ) with a scan rate of 0.02° s^{-1}.

Specific surface areas were determined by BET formalism for the calcined Mg*x*Al–O samples. Nitrogen adsorption and desorption isotherms were obtained to determine pore size distribution using BJH method. The analyses were performed at −196 °C in a Micromeritics ASAP 2020 equipment.

Surface basicity was investigated by temperature-programmed desorption of CO_2 (TPD-CO_2) carried out in an AutoChem II equipment from Micromeritics. The samples were initially treated at 500 °C under a stream of 8% O_2/He (vol.%) at 50 mL min^{-1} in order to eliminate eventual carbonated species generated by air exposure during handling and storage ensuring thus the surface cleanness. After, they were cooled to room temperature and then were submitted to a flow of pure CO_2 for 30 min. Lastly, the reactor was purged with He prior to the thermal desorption analyses. The desorption profiles were collected using a He flow of 50 mL min^{-1} and rising the temperature up to 1000 °C, following a 10 °C min^{-1} linear temperature ramp.

Chemical composition of all samples was determined by X-ray fluorescence spectrometry carried out in a Bruker S8 Tiger spectrometer.

2.4. Catalytic evaluation

Catalytic activity and stability were evaluated on steam reforming of glycerol in a continuous flow system equipped with a fixed-bed stainless steel tubular reactor with ϕ = 12 mm. In a typical test, before the reaction, 40 mg of the powdered catalyst was mixed with an inert material to avoid any temperature gradient in the catalytic bed. It was reduced *in situ* at 600 °C for 1 h under pure hydrogen. A syringe pump was used to feed the reactor with the glycerol solution (36 wt.%) at 0.13 mL min^{-1}. The liquid was vaporized in the first third of the reactor. This feed stream was diluted with a 172 mL min^{-1} flow of a nitrogen/argon mixture. A contact time of 511 h^{-1} was used in all tests with a water to glycerol molar ratio in the gas phase of 9:1, at 600 °C and at atmospheric pressure.

The gaseous products were analyzed on-line by TCD and FID detectors in an Agilent 7890A GC chromatograph. A CarboxenTM 1010 Plot (30 m × 0.530 mm) column was employed to determine N_2, H_2, CO, CO_2, CH_4 and C_2H_4. Regarding the liquid phase products, the stream was continuously condensed and the concentration of unreacted glycerol and the distribution of the products in the liquid phase were further determined by high performance liquid chromatography (HPLC) on a Waters Alliance e2695 equipment coupled to a refractive index detector (RID). The analyses were performed in isocratic elution mode, using an aqueous H_2SO_4 solution at 0.05 mol L^{-1} as eluent at 0.7 mL min^{-1} and a Biorad Aminex HPX-87H ion exchange column. The temperatures of the column and RID were kept at 65 and 50 °C, respectively.

Global conversion of glycerol (X_{global}) was calculated based on glycerol concentration in the initial solution (F^{in}) and in the condensed phase from the reactor outlet (F^{out}):

$$X_{global}\ (\%) = \frac{F_{gly}^{in} - F_{gly}^{out}}{F_{gly}^{in}} \times 100$$

Glycerol conversion to gaseous products (X_{gas}) was determined from the molar flow of the non-condensable products in the outlet (F_i) and the glycerol molar flow in the inlet:

$$X_{gas}(\%) = \frac{F_{CH_4} + 2F_{C_2H_4} + F_{CO_2} + F_{CO}}{3F_{gly}^{in}} \times 100$$

Selectivity data was calculated by applying the following equations:

$$S_{H_2}(\%) = \frac{3}{7} \times \frac{F_{H_2}}{F_{CO_2} + F_{CO} + F_{CH_4} + 2F_{C_2H_4}} \times 100$$

$$S_i(\%) = \frac{F_i}{F_{CO_2} + F_{CO} + F_{CH_4} + 2F_{C_2H_4}} \times 100$$

2.5. Characterization of used catalysts

The used catalysts were collected after the reaction and characterized in order to shed some light on the eventual deactivation process. Temperature-programmed oxidation (TPO) was performed in a TA Instruments SDT Q600 thermobalance coupled to an Ametek quadrupolar mass spectrometer (TPO/TGA-MS). The analyses were conducted following a heating rate of 20 °C min^{-1} up to 900 °C under synthetic air at 50 mL min^{-1}.

Finally, the used catalysts were ultrasonically suspended in isopropanol and deposited on a carbon-coated copper grid for Transmission Electron Microscopy (TEM) examination using a Tecnai 20 FEI microscope.

3. Results and discussion

3.1. Characterization of supports and catalysts

3.1.1. X-ray diffraction of synthesized supports

The diffraction patterns of the prepared LDH (Mg5Al–H and Mg3Al–H) show that lamellar structures were indeed formed (Fig. 1), irrespective of their chemical composition. Nevertheless, the solids with different Mg/Al ratios exhibit an expected shift in the position of the peaks due to the slight variation of the interlayer spacings, being 0.797 and 0.818 nm for Mg5Al–H and

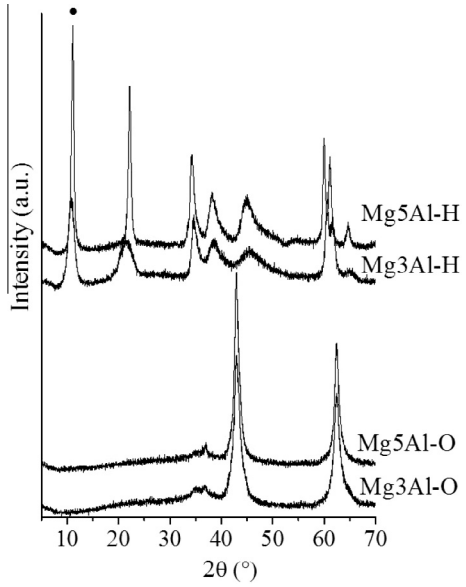

Fig. 1. XRD patterns of the synthesized supports.

Table 1
BET surface area (S_{BET}) and density of surface basic sites calculated for the resulting mixed oxides.

Support	S_{BET} (m^2/g)	Basic sites			
		Weak (%)	Medium (%)	Strong (%)	Total (μmol/m^2)
Mg5Al–O	140	18	9	73	440
Mg3Al–O	149	22	17	61	334

Mg3Al–H, respectively. Such a shorter spacing upon the increase of the Mg/Al ratio is a consequence of the layer charge decrease as well as the gallery height. Yet, the separation between the layers is also determined by the dimensions of the anions guested within the interlamellar space. Either interlayer distances revealed by the XRD profiles will correspond approximately to an average value if the presence of both $[NO_3]^-$ (0.879 nm) and $[CO_3]^{2-}$ (0.765 nm) [29] anions are considered within the interlamellar domain. It suggests that some CO_2 was still dissolved in the aqueous solution despite the constant N_2 flushing during co-precipitation, finding its way into the interlayer space. The broader reflections noticed in Mg3Al–H pattern when compared with Mg5Al–H indicate a less ordered structure or the formation of smaller crystallites as already observed for other Mg-rich hydrotalcite type materials [36]. Lastly, the diffractograms show no evidence of any crystalline $Mg(OH)_2$ or $Al(OH)_3$ phases.

Regarding the structure of the calcined samples, also depicted in Fig. 1, it can be seen that the heat treatment leads to the formation of oxides phases, herein identified as Mg3Al–O and Mg5Al–O. The diffractograms essentially exhibit, however, reflections only associated with MgO cubic phase, which is ascribed to the pretty high Mg/Al ratios in both solids. The patterns do not show any sign of the presence of an Al_2O_3 crystalline phase. In fact, an amorphous halo between 20° and 30°, which is typical of materials with low crystallinity, is easily noted and may be related to a segregated transition Al_2O_3 phase. It is thus conceivable that $MgO{\cdot}Al_2O_3$ mixed oxides powders are obtained.

3.1.2. Porosity of synthesized supports

BET areas of the two oxide samples are collected in Table 1. It is seen that these solids present high surface areas as expected for this sort of materials derived from layered double hydroxides [29,37]. It is also noted that the values are pretty similar irrespective of the Mg/Al ratio. However, some textural disparities arise when analyzing their N_2 isotherms and BJH desorption pore diameter distributions as depicted in Fig. 2.

It is seen that the isotherms present different features. Mg3Al–O exhibits typical type IV isotherm with a broad H1 type hysteresis loop, indicating the occurrence of mesopores. On the other hand, the sample with higher Mg/Al ratio (Mg5Al–O) shows a type II isotherm, the normal form obtained with macroporous/non-porous materials. These pore differences are consistently clear in their diameter distributions (Fig. 2).

3.1.3. Basic properties of synthesized supports

As a discussion on the role of the basic properties of the catalysts on their performance and stability is one of the goals of this work, TPD experiments using CO_2 as an acidic probe molecule were made but only for the two calcined samples, since they are the only samples thermally stable enough. The results indicate a wide distribution of basic surface sites as displayed by the large temperature range of the desorption peaks in the profiles in Fig. 3. These data were used to quantitatively determine the total amount of basic centers as well as to distinguish the surface sites according

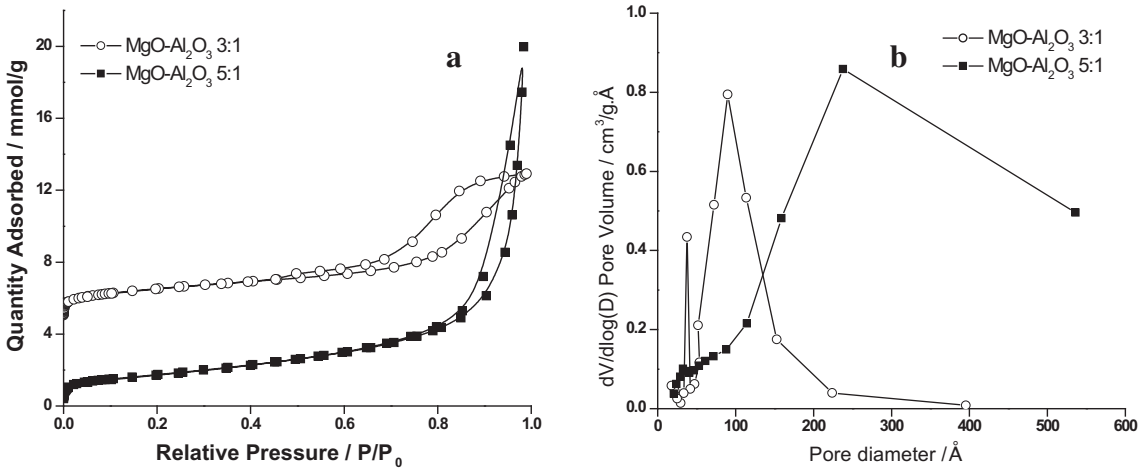

Fig. 2. N_2 isotherms (a) and pore diameter distribution (b) of the calcined mixed oxides.

to their basicity strength. The density of basic surface sites was normalized by surface area considering the BET results reported and discussed hereinbefore.

The records summarized in Table 1 show some differences in the total amount of basic sites, the mixed oxide with higher magnesium content being the more basic solid. For a more detailed investigation of each type of surface center, desorption peaks below 250 °C were considered as corresponding to a moderate to weak basicity. Above this temperature, CO_2 release is a consequence of the existence of strong basic sites. Taking into account these indications, the amount of CO_2 detected for each sample was calculated and classified as exhibited in Table 1. These data along with the wide range of temperature at which desorption occurs show that the two solids are described by a major population of strong sites. This is even more significant for the sample containing higher magnesium loading (Mg5Al–O), indicating that it has a predominant concentration of low coordination O^{2-} anions [37]. On the other hand, sample Mg3Al–O carries more sites classified as moderate or weak basic centers than sample Mg5Al–O, respectively 39% and 27% of the total amount.

3.1.4. Chemical composition of fresh catalysts

The metal catalysts obtained either from impregnation of LDH or mixed oxide solids were essentially characterized as regarding their chemical composition. The results show that the catalysts possess similar metal loadings and that the experimental Mg/Al ratios are in good agreement with the theoretical ones (Table 2).

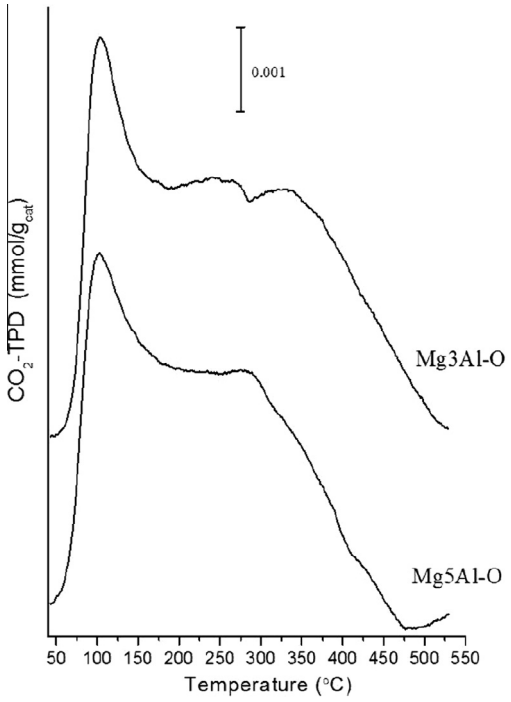

Fig. 3. TPD-CO_2 profiles of the mixed oxides.

Table 2
Chemical composition of the supported catalysts.

Catalyst	Pt (wt.%)	Mg/Al
PtMg5Al–H	1.4	5.0
PtMg3Al–H	1.3	3.5
PtMg5Al–O	1.2	5.6
PtMg3Al–O	0.9	3.2

3.2. Catalytic activity

3.2.1. Global and gas conversion

All supported catalysts were tested for the steam reforming of glycerol and the gaseous products were analyzed firstly to infer on their effectiveness for hydrogen generation. The distribution of products in the gas phase is depicted in Table 3, revealing that indeed high concentrations of H_2 and CO_2 were formed with maximum selectivities to H_2 of ~68%. It is interesting to note that H_2 and CO_2 selectivities are higher for those catalysts exhibiting lower Mg/Al ratio. Still, the presence of CO and a very low concentration of hydrocarbons (ethylene, ethane and methane) are also detected for all the catalysts tested. This gas composition is in close agreement with those reported so far for a multitude of different catalyst composition [38]. It should be mentioned, however, that H_2 selectivity reached herein (<70%) is slightly lower than those usually reported for non-noble metal catalysts (70–80%) [38].

Examining the data summarized in Table 3, it is possible to learn that the H_2/CO_2 ratio is similar for the four catalysts. The calculated values for this ratio satisfactorily approach the theoretical value (H_2/CO_2 = 2.3) attributed to the reforming reaction (Eq. (1)). Consequently, under the chosen conditions, we can conclude that the two families of LDH-derived catalysts can indeed convert glycerol to hydrogen through steam reforming reaction.

Fig. 4 shows the global glycerol conversion at 600 °C as a function of time on stream to estimate catalytic activity and stability of the four catalysts. The temperature of these experiments took into consideration the fairly low contribution of homogeneous thermal conversion of glycerol as previously determined from blank tests [39]. By observing Fig. 4, it is easy to note that the most stable sample is the catalyst PtMg5Al–H, which exhibits an almost constant conversion of about 85%. Having a similar synthesis approach, catalyst PtMg3Al–H reaches a similar glycerol conversion of 80% at the very beginning of the reaction run; however, it undergoes a severe deactivation causing the conversion to drop gradually reaching 20% after 6 h. The other samples, produced through the impregnation of the mixed oxides, present lower activities. Still, they delineate a marked deactivation trajectory too, beginning with glycerol conversions of 55–65% and decreasing steadily along the 6 h until accomplishing only 25%. Although these two mixed oxide-supported catalysts have poorer performances, it is interesting to observe that the one with the highest Mg/Al ratio consistently accomplish and maintain higher glycerol conversion. It is thus plainly seen that the catalysts mostly differ in their resistance to deactivation.

The gas conversion (X_{gas}) depicted in Fig. 5 is an important parameter for the analysis of the H_2 yield in glycerol reforming. Concerning these calculations, samples of the "H" family behave similarly with an average value of 35% after the first hour and reaching 25–30% at the end of the experimental run. Sample PtMg5Al–O exhibits a consonant behavior, excepting it achieves ~20% within the same reaction period. On the other hand, PtMg3Al–O presents the most stable curve but with a quite low

Table 3
Gas phase selectivities and carbon balances of the catalysts tested in glycerol reforming at 600 °C.

Catalyst	Selectivity (%)				$\frac{H_2}{CO_2}$	Carbon balance[b] (%)
	H_2	CO_2	CO	HC[a]		
PtMg5Al–H	48.5	50.0	9.7	2.3	2.3	98
PtMg3Al–H	65.0	67.9	10.2	2.4	2.2	91
PtMg5Al–O	51.8	53.0	10.6	3.7	2.3	94
PtMg3Al–O	68.2	59.5	27.0	14.5	2.6	82

[a] HC = hydrocarbons: ethane, ethylene and methane.
[b] Carbon balance considering only gaseous and liquid products.

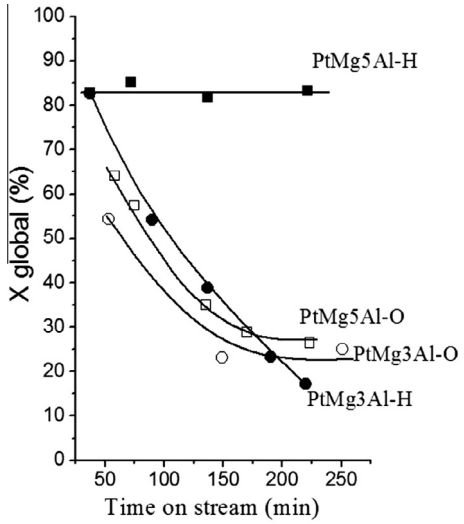

Fig. 4. Glycerol global conversion (X_{global}) during time on stream for steam reforming reaction at 600 °C.

gaseous conversion of only 5%. Preliminarily, it is reasonable to say that these results show that the "O" family catalysts are less efficient than the "H" family.

Compare and contrast global glycerol conversion (X_{global}) and gaseous conversion (X_{gas}) should lead to a sharp evaluation of the catalyst performance. The results presented herein indicated that sample PtMg5Al–H is the most active as regarding global conversion. Nonetheless, the catalyst PtMg3Al–H is to be appointed as the most effective for the production of H_2 since the two calculated conversions – X_{global} and X_{gas} – resulted in quite similar values. In other words, by using this catalyst, all glycerol consumed is converted into gas products, primarily hydrogen and CO_2. Therefore, the catalyst PtMg3Al–H produces a lower concentration of organic by-products in liquid phase, which might be correlated to its lower density of strong basic sites as discussed previously. Again, focusing squarely on such compare-and-contrast examination, catalysts synthesized by the direct impregnation of the layered double hydroxides ("H" family) led to a better catalytic behavior.

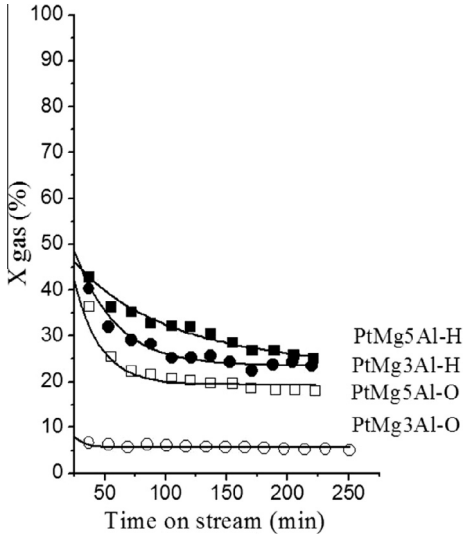

Fig. 5. Conversion to gaseous products (X_{gas}) during time on stream for glycerol steam reforming reaction at 600 °C.

As for the catalyst PtMg5Al–H, the physico-chemical characterization along with its catalytic evaluation suggests that the higher population of strong basic sites favors the initial steps of the reaction. In fact, it is generally accepted that the strength of the basic site is one of the determining features to influence the abstraction of H atoms through a dehydrogenation route. Consequently, this chemical property associated with the presence of metal sites is possibly responsible for the high X_{global} observed for sample PtMg5Al–H. However, as mentioned before and contrarily to the objective of the overall reforming reaction, the glycerol conversion toward liquid products is high (~60%). This means that parallel reactions were markedly promoted leading to the formation of by-products, which constitute the major components of the reaction output from this catalyst. On the other hand, the catalytic results obtained for sample PtMg3Al–H indicate that its weak to moderate basicity leads to a more selective catalytic performance. As concerning acid–base properties, it is usually accepted that besides the strength of the acid sites, a narrow or more balanced distribution of basic strength is also desired; otherwise the selectivity and the stability may be strongly affected [40]. Unfortunately, fundamental studies on basic properties in catalyzed reactions are not as developed as the acid ones yet and much is still to be done. Nonetheless, it is well agreed that the strength of basic sites required for base-catalyzed reactions, or a base-catalyzed reaction step as in glycerol reforming, varies with the easiness of proton abstraction from the reactant molecule under the reaction conditions employed [41]. This fashion has indeed been claimed in glycerol reforming studies at which different acid/basic supports have been used and acid solids have consistently failed to render effective catalysts [4]. Nonetheless, it has been demonstrated that the use of basic materials does not solely assure the stability of the catalyst for glycerol steam reforming [38]. This is because dehydration on dual sites (basic oxygen centers and coordinatively unsaturated cations acting as Lewis acid sites) on the support surface can still provoke the formation of undesired coke precursors [3].

3.2.2. Distribution of products in liquid phase

For a deeper discussion and further understand the reaction pathways occurring under the operation conditions followed here, the distribution of products in liquid phase was also examined. To proceed this investigation, around six aliquots from the condensate were collected at regular intervals of time and analyzed by HPLC. Fig. 6 shows the distribution of products as a function of the reaction time for both "H" catalysts, PtMg5Al–H and PtMg3Al–H, which had the more interesting and contrastive performances regarding global activity.

The results indicate a similar trend for both catalysts showing the production of the same set of compounds with the prominent presence of acetol, pyruvaldehyde and lactic acid. Indeed, these products have been recently detected by some other authors [19], but in different proportion comparing to this contribution. It is interesting to mention though that the authors applied milder conditions considering this present work. For example, a residence time of 7.50 g_{cat} h/$mol_{glycerol}$ was used while we have applied a much lower value (1.25 g_{cat} h/$mol_{glycerol}$), which should accelerate catalyst deactivation. On the other hand, they adopted a lower reaction temperature (350 °C) and obtained a global conversion of 75% and a gaseous conversion of 46% [19]. Those conditions led to the formation of ethylene glycol, dihydroxyacetone and acetaldehyde as main products. Yet, acetol and pyruvaldehyde were produced in very low concentrations. That distribution of products was also related to the neutral character of the support used (SiO_2) which should not favor the dehydration route [19].

Unfortunately, very few articles [42] reveal the composition of the liquid products while studying glycerol reforming and much

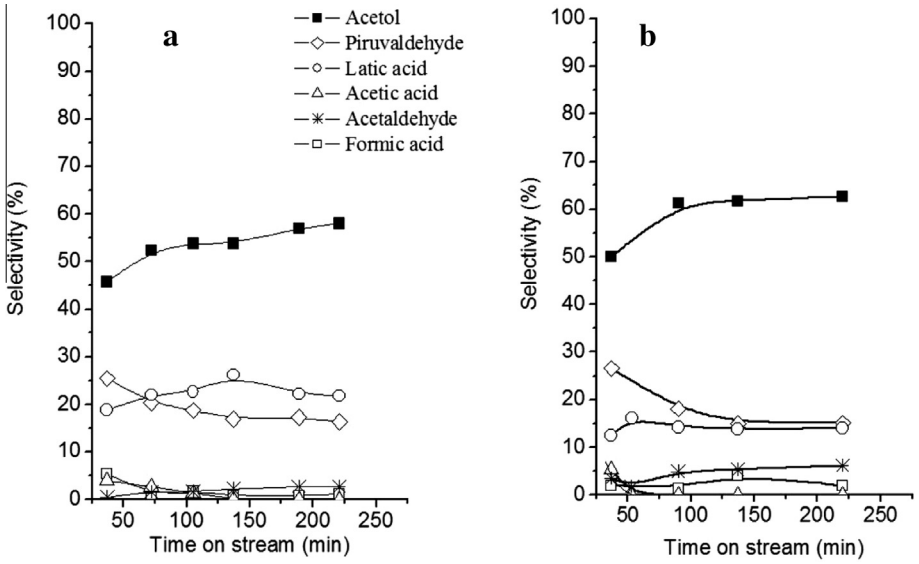

Fig. 6. Molar composition of liquid products as a function of time on stream for catalysts PtMg5Al–H (a) and PtMg3Al–H (b).

are still to be done. In the case of the present catalysts derived from LDH, it can be suggested that the major concentration of strong basic sites contributes to the sequence of reactions depicted in Scheme 1.

The proposed reaction pathway over the metal and basic sites on the studied catalysts starts with glycerol dehydrogenation, followed by a dehydration step leading to pyruvaldehyde; all steps proceeding on the support surface sites. Finally, pyruvaldehyde may be converted to acetol (hydroxyacetone) through hydrogenation over the metal sites and lactic acid, which was possibly produced by the Cannizzaro rearrangement due to the catalyst basicity. Aldehyde decarbonylation from cleavage of C–C bonds would generate the gaseous products. As a deactivation process was observed (Fig. 4), the breakage of C–O bonds in adsorbed intermediates has also to be considered, which would generate carbon deposits. Condensation of those reactive organic intermediate compounds into heavy carbonaceous materials may not be ruled out though.

Finally, it should be highlighted that the carbon balance considering gas and liquid products is quite satisfactory as presented in Table 3. The difference observed is roughly consistent with total amount of carbon deposited on each catalyst as seen by the absolute values determined for each catalytic run (not shown).

3.2.3. Characterization of used catalysts

To understand the nature of the carbon deposits, some characterization techniques were applied to investigate the used catalysts.

TPO/TGA-MS analyses showed to be a valuable experiment to progress the post-reaction studies. Profiles revealed different thermal events, followed by the evolution of CO_2 ($m/z = 44$) as disclosed by coupled mass spectrometer as depicted in Fig. 7. It also shows the derivatives curves of the mass loss (dTG). According to dTG curves, there are three thermal events in the analysis of all four used catalysts. The first one takes place in the initial stages of the temperature rise up to 150 °C and can be solely attributed to the loss of water as observed by mass spectrometry. The second and third thermal events are more or less resolved depending on the sample, covering a wide range of temperature. The corresponding CO_2 profiles (Fig. 7, dashed lines) confirm that such mass loss is

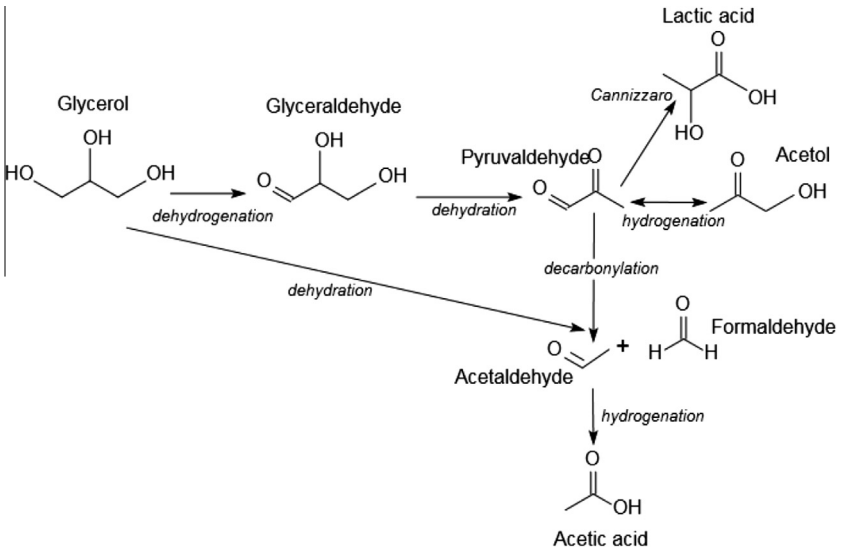

Scheme 1. Reaction pathway to organic liquid products from glycerol.

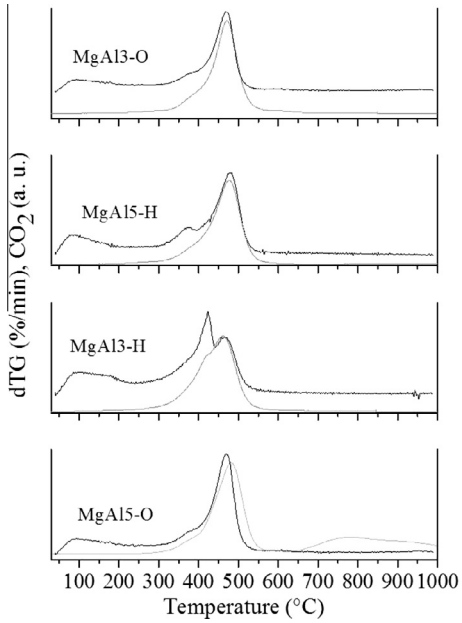

Fig. 7. TPO profiles of the catalysts after steam reforming of glycerol at 600 °C.

a consequence of the gasification of carbon deposits on the samples. Interestingly, apart from the previously described contribution at low temperature (<200 °C), water (m/z = 18) was only evolved as a tiny peak between 380 and 420 °C for all samples (not shown). This finding suggests that the residues may contain slightly different carbon species, leading to either CO_2 and water or only CO_2 as gasification products.

By deconvoluting the main dTG unresolved broadened peak, it is indeed possible to note that the CO_2 evolution profile comprises three components that have maxima ranging approximately between 345–425 °C (A1), 425–440 °C (A2) and 455–490 °C (A3), as can be observed in the representative curves displayed in Fig. 8. The first peak A1 perfectly matches the temperature range at which water is also released, indicating that the parent CO_2 discharge results from the decomposition/burn off of remaining organic compounds ($C_xH_yO_n$) adsorbed on the catalysts along reaction. The other components attached only to CO_2 formation can thus be attributed to gasification of carbon species (C).

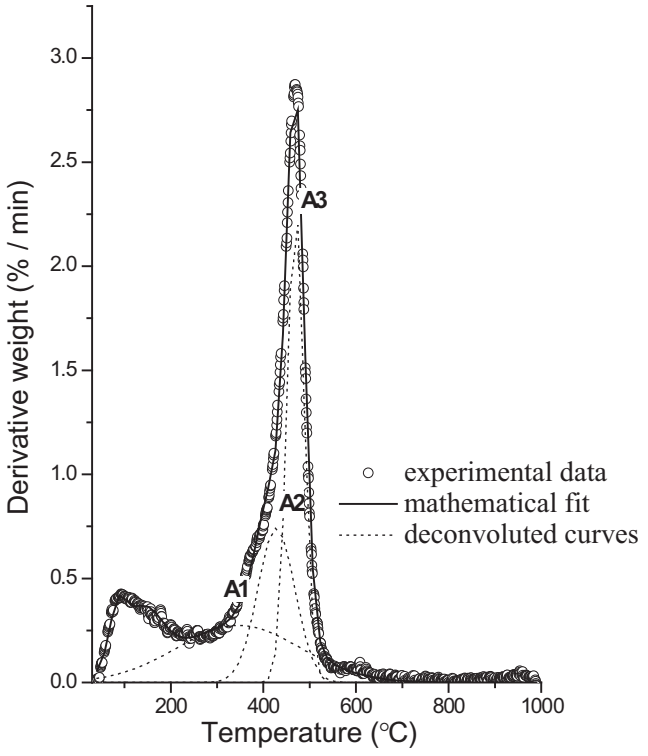

Fig. 8. Deconvoluted TPO profile of PtMg3Al–O catalyst.

By calculating the global weight loss associated with all carbonaceous species (excluding thus that below 200 °C) and discriminating every single contribution (associated with each of the three deconvoluted peaks), it is possible to make some assumptions. For a more realistic approach, those amounts of carbon were analyzed separately normalized by the catalyst mass, Pt loading and the global glycerol conversion (final conversion). These values are summarized in Table 4. It should be firstly noted that the amount of coke deposited on these Pt catalysts (10–15 wt.%) are higher than those reported elsewhere (2–12 wt.%) [19,21]. It is probably associated with the higher concentration of basic surface sites on the samples in this study as previously discussed herein. It can also be seen that the total amount of coke does satisfactorily correlates with the catalyst stability. However, such a trend cannot be equally expressed by all deconvoluted fractions. It might thus suggest that they are not evenly responsible for the global deactivation process.

In order to make it clearer, the contents of the different coke fractions were correlated with the percentage of deactivation (difference between the initial and the final conversions) of each catalyst (Fig. 9). As it can be seen through the evaluation of the coefficient of determination (R^2), a more satisfactory correlation between carbon amount and degree of deactivation was found for the more stable carbon species, those corresponding to peak A3 at higher temperatures. This indicates that the more reactive carbon species, which give rise to peaks A1 and A2, have minor participation on the deactivation process of the catalysts. This is an opposite proposition to that ~~of~~ presented elsewhere [19], which relied on results obtained at mild conditions (lower temperature and higher residence time). In that case, the authors concluded that deactivation was caused by reaction intermediates adsorbed on the catalyst, and responsible for generating the peaks at very low temperatures in TPO experiments [19].

As already emphasized hereinbefore, the nature of deactivating carbon sources has only recently been studied for glycerol reforming [19,20,39,43,44] and a profitable discussion has to be motivated. Additionally, they are especially scarce for platinum based catalysts [3,19,21,22,38,45,46]. This recent literature reflects the complexity and variation of carbon species in the light of the well-documented knowledge on the mechanism of coke formation involved in methane, ethanol and other oxygenated compounds steam reforming [47–51]. It is thus generally accepted that carbon

Table 4
Amounts of carbon deposited on used catalysts as calculated from TPO/TGA-MS analyses.

Catalyst	Total carbon content (wt.%)	Normalized total carbon content[a]	C_{A1}[b]	C_{A2}[b]	C_{A3}[b]
PtMg5Al–H	10.0	0.0026	0.0010	0.0008	0.0008
PtMg3Al–H	12.6	0.0134	0.0066	0.0036	0.0032
PtMg5Al–O	14.5	0.0064	0.0023	0.0021	0.0020
PtMg3Al–O	12.0	0.0051	0.0017	0.0014	0.0020

[a] Total mass loss above 200 °C as normalized by the catalyst mass, the global glycerol conversion and Pt loading.
[b] Mass loss corresponding to fractions A1, A2 and A3 according to the deconvolution of dTG curves as defined in Fig. 8.

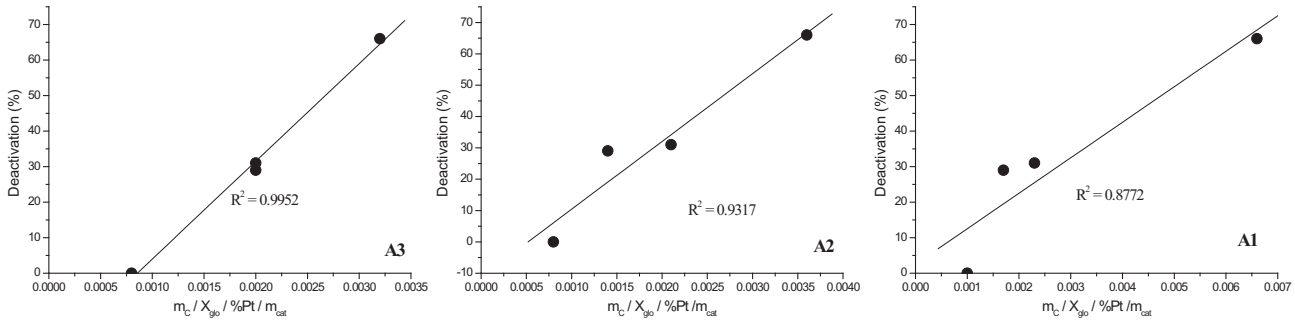

Fig. 9. Correlation between the amount of carbon deposits (areas A1, A2, A3 as defined in Fig. 7) and catalyst deactivation.

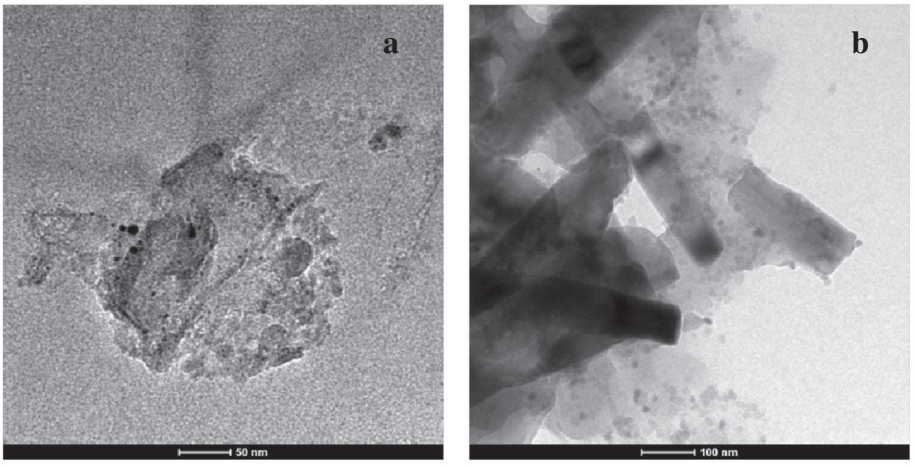

Fig. 10. TEM images of used PtMg5Al–H (a) and PtMg5Al–O (b) catalysts.

deposition during glycerol steam reforming present different reactivity, associated with more stable polymeric or more reactive carbon species [20]. For example, the source of the deactivation process is often claimed to be: side reactions as the Boudouard reaction and methane decomposition [52] and glycerol adsorption or the presence of intermediate products generated by glycerol dehydration/dehydrogenation (unsaturated coke precursors) [3,7,38,44]. As regarding the formation of reactive organic intermediates, acid–base surface properties of catalysts have been considered to play important role on coke formation for Pt supported materials [10,19,38]. In the present study, side products were indeed identified through liquid phase analysis. It is important to remember that hydrotalcite type materials present acid Lewis sites (coordinatively unsaturated cations) along with basic properties [53]. This certainly contributed to the formation of condensed compounds, which may not eventually be reformed to produce gas products as very recently suggested elsewhere [54]. If so, the acid–base sites could keep dehydrogenating the organic species. It would thus ultimately lead to the formation of those more stable carbon deposits similarly to the well-accepted coke formation mechanisms for other oxygenated compounds such as ethanol and bio-oil [38]. However, the desorption of those intermediates from the catalyst surface to the outlet gas stream should also be considered. In this case, the formation of oxygenated by-products would not affect the catalyst performance. Taking into account all these propositions, our findings suggest that the intermediate compounds are not the ones to be straightforwardly credited with deactivation. Any contribution from these compounds to carbon formation would thus be indirect.

On the other hand, sintering of platinum particles is mostly limited to APR conditions [21,45], although it has also been considered a secondary cause for catalyst deactivation in glycerol steam reforming [55]. As concerning the metal role, it shall also be considered that low gasification temperatures may be associated with carbon deposits near metallic centers while higher temperature ones correspond to carbon deposited on the support [56].

The remarkable stability of PtMg5Al–H catalyst may be indeed associated with its high metal dispersion, which would facilitate *in situ* carbon decomposition/burn off during the reaction. The preparation method applied to obtain "H" samples has already been confirmed as a way to promote high metal dispersion [33]. In order to verify eventual differences in the catalysts dispersion, the spent catalysts were examined by TEM (Fig. 10). It was seen that sample PtMg5Al–H indeed exhibits an average particle diameter lower than its counterpart catalyst PtMg5Al–O. While Pt nanoparticles with 3 nm is present in PtMg5Al–H after glycerol steam reforming reaction, much larger ones (13 nm) is observed on PtMg5Al–O. It is important to recall that TEM examination was limited to metal dispersion due to the presence of an inert material mixed with the catalyst to avoid any temperature gradient along reaction.

It is interesting to highlight at this point, as hydrotalcite type materials are frequently used in catalytic studies, that a simple change in the preparation procedure can lead to a completely different behavior, to catalysts with distinct characteristics even when the same chemical composition is used, and better catalytic results can be accomplished. The different basicity of the supports, tailored by their Mg/Al ratio and synthesis procedure, clearly affected its selectivity to H_2. The catalysts bearing weak to moderate basic sites

(PtMg3Al) showed the highest H_2 production, while those with strong basic centers led to the formation of liquid oxygenated compounds. This fashion was comparable to the resistance to deactivation of the catalysts, with the PtMg3Al samples being more stable than the other PtMg5Al group. It corroborated the suggestion that the formation of oxygenated by-products might play a secondary role in deactivation. Finally, a more dispersed catalyst, which may also be showed to play a role in catalyst surface cleanness.

4. Conclusion

Pt catalysts supported on layered double hydroxide and the derived mixed oxides were studied in glycerol steam reforming. All catalysts showed to be active but the one synthesized directly from the layered double hydroxide precursors with Mg/Al ratio of 3 revealed to be more effective. For this catalyst, global and gas conversion were similar and varied within 60–25%. The presence of weak to moderate basic surface sites rendered more selective catalysts, accomplishing up to 68% selectivity to hydrogen. Deactivation was observed on all catalysts irrespective their Mg/Al molar ratio. The more stable carbon deposits played the major role in the deactivation process. Carbonaceous materials derived from intermediate organic liquid compounds also took a part in deactivation but with only a minor contribution. Highly dispersed metal centers showed to be important for *in situ* catalyst surface cleanness.

Acknowledgements

PROSUL/CNPq 490187/2010-2 (Brazil) is acknowledged for financial support and fellowships. The authors thank Ms. Nataly Amorim from CETENE (Brazil) for TEM analyses.

References

[1] R.D. Cortright, R.R. Davda, J.A. Dumesic, Hydrogen from catalytic reforming of biomass-derived hydrocarbons in liquid water, Nature 418 (2002) 964–967.
[2] G.W. Huber, J.W. Shabaker, J.A. Dumesic, Raney Ni–Sn catalyst for H_2 production from biomass-derived hydrocarbons, Science 300 (2003) 2075–2077.
[3] R.R. Soares, D.A. Simonetti, J.A. Dumesic, Glycerol as a source for fuels and chemicals by low-temperature catalytic processing, Angew. Chem. Int. Ed. 45 (2006) 3982–3985.
[4] A.O. Menezes, M.T. Rodrigues, A. Zimmaro, L.E.P. Borges, M.A. Fraga, Production of renewable hydrogen from aqueous-phase reforming of glycerol over Pt catalysts supported on different oxides, Renewable Energy 36 (2011) 595–599.
[5] H.C. Lee, K.W. Siew, J. Gimbun, C.K. Cheng, Synthesis and characterisation of cement clinker-supported nickel catalyst for glycerol dry reforming, Chem. Eng. J. 255 (2014) 245–256.
[6] D.A. Simonetti, E.L. Kunkes, J.A. Dumesic, Gas-phase conversion of glycerol to synthesis gas over carbon-supported platinum and platinum–rhenium catalysts, J. Catal. 247 (2007) 298–306.
[7] S. Adhikari, S. Fernando, A. Haryanto, A comparative thermodynamic and experimental analysis on hydrogen production by steam reforming of glycerin, Energy Fuels 21 (2007) 2306–2310.
[8] A.M.D. Douette, S.Q. Turn, W. Wang, V.I. Keffer, Experimental investigation of hydrogen production from glycerin reforming, Energy Fuels 21 (2007) 3499–3504.
[9] M.L. Dieuzeide, V. Iannibelli, M. Jobbagy, N. Amadeo, Steam reforming of glycerol over Ni/Mg/γ-Al_2O_3 catalysts. Effect of calcination temperatures, Int. J. Hydrogen Energy 37 (2012) 14926–14930.
[10] F. Pompeo, G. Santori, N.N. Nichio, Hydrogen and/or syngas from steam reforming of glycerol. Study of platinum catalysts, Int. J. Hydrogen Energy 35 (2010) 8912–8920.
[11] C. Wang, B. Dou, H. Chen, Y. Song, Y. Xu, X. Du, T. Luo, C. Tan, Hydrogen production from steam reforming of glycerol by Ni–Mg–Al based catalysts in a fixed-bed reactor, Chem. Eng. J. 220 (2013) 133–142.
[12] S. Adhikari, S. Fernando, A. Haryanto, Production of hydrogen by steam reforming of glycerin over alumina-supported metal catalysts, Catal. Today 129 (2007) 355–364.
[13] S. Czernik, R. French, C. Feik, E. Chornet, Hydrogen by catalytic steam reforming of liquid byproducts from biomass thermoconversion processes, Ind. Eng. Chem. Res. 41 (2002) 4209–4215.
[14] T. Hirai, N. Ikenaga, T. Miyake, T. Suzuki, Production of hydrogen by steam reforming of glycerin on ruthenium catalyst, Energy Fuels 19 (2005) 1761–1762.
[15] E.L. Kunkes, R.R. Soares, D.A. Simonetti, J.A. Dumesic, An integrated catalytic approach for the production of hydrogen by glycerol reforming coupled with water–gas shift, Appl. Catal. B 90 (2009) 693–698.
[16] B. Zhang, X. Tang, Y. Li, Y. Xu, W. Shen, Hydrogen production from steam reforming of ethanol and glycerol over ceria-supported metal catalysts, Int. J. Hydrogen Energy 32 (2007) 2367–2373.
[17] S. Adhikari, S. Fernando, S. To, R.M. Bricka, P.H. Steele, A. Haryanto, Conversion of glycerol to hydrogen via a steam reforming process over nickel catalysts, Energy Fuels 22 (2008) 1220–1226.
[18] A. Iriondo, V.L. Barrio, J.F. Cambra, P.L. Arias, M.B. Guemez, R.M. Navarro, Hydrogen production from glycerol over nickel catalysts supported on Al_2O_3 modified by Mg, Zr, Ce or La, Top. Catal. 49 (2008) 46–58.
[19] F. Pompeo, G.F. Santori, N.N. Nichio, Hydrogen production by glycerol steam reforming with Pt/SiO_2 and Ni/SiO_2 catalysts, Catal. Today 172 (2011) 183–188.
[20] C.K. Cheng, S.Y. Foo, A.A. Adesina, Carbon deposition on bimetallic Co–Ni/Al_2O_3 catalyst during steam reforming of glycerol, Catal. Today 164 (2011) 268–274.
[21] A. Ciftci, B. Peng, A. Jentys, J.A. Lercher, E.J.M. Hensen, Support effects in the aqueous phase reforming of glycerol over supported platinum catalysts, Appl. Catal. A 431–432 (2012) 113–119.
[22] N.J. Luo, J.A. Wang, T.C. Xiao, F.H. Cao, D.Y. Fang, Influence of nitrogen on the catalytic behaviour of Pt/γ-Al_2O_3 catalyst in glycerol reforming process, Catal. Today 166 (2011) 123–128.
[23] M.L. Dieuzeide, N.E. Amadeo, Thermodynamic analysis of glycerol steam reforming, Chem. Eng. Technol. 33 (2010) 89–96.
[24] V.V. Thyssen, T.A. Maia, E.M. Assaf, Ni supported on La_2O_3–SiO_2 used to catalyze glycerol steam reforming, Fuel 105 (2013) 358–363.
[25] J.R. Mawdsley, T.R. Krause, Rare earth-first-row transition metal perovskites as catalysts for the autothermal reforming of hydrocarbon fuels to generate hydrogen, Appl. Catal. A 334 (2008) 311–320.
[26] K.F.M. Elias, A.F. Lucredio, E.M. Assaf, Effect of CaO addition on acid properties of Ni–Ca/Al_2O_3 catalysts applied to ethanol steam reforming, Int. J. Hydrogen Energy 38 (2013) 4407–4417.
[27] A. Romero, M. Jobbágy, M. Laborde, G. Baronetti, N. Amadeo, Ni(II)–Mg(II)–Al(III) catalysts for hydrogen production from ethanol steam reforming: influence of the activation treatments, Catal. Today 149 (2010) 407–412.
[28] A. Romero, M. Jobbágy, M. Laborde, G. Baronetti, N. Amadeo, Ni(II)–Mg(II)–Al(III) catalysts for hydrogen production from ethanol steam reforming: influence of the Mg content, Appl. Catal. A 470 (2014) 398–404.
[29] F. Cavanni, F. Trifiró, A. Vaccari, Hydrotalcite-type anionic clays: preparation, properties and applications, Catal. Today 11 (1991) 173–301.
[30] A.J. Vizcaíno, P. Arena, G. Baronetti, A. Carrero, J. Calles, M. Laborde, N. Amadeo, Ethanol steam reforming on Ni/Al_2O_3 catalysts: effect of Mg addition, Int. J. Hydrogen Energy 33 (2008) 3489–3492.
[31] H. Morioka, Y. Shimizu, M. Sukenobu, K. Ito, E. Tanabe, T. Shishido, K. Takehira, Partial oxidation of methane to synthesis gas over supported Ni catalysts prepared from Ni–Ca/Al-layered double hydroxide, Appl. Catal. A 215 (2001) 11.
[32] K. Tomishige, S. Kanazawa, K. Suzuki, M. Asadullah, M. Sato, K. Ikushima, K. Kunimori, Effective heat supply from combustion to reforming in methane reforming with CO_2 and O_2: comparison between Ni and Pt catalysts, Appl. Catal. A 223 (2002) 35–42.
[33] S. Narayanan, K. Krishna, Structure activity relationship in Pd/hydrotalcite: effect of calcination of hydrotalcite on palladium dispersion and phenol hydrogenation, Catal. Today 49 (1999) 57–63.
[34] H.J. Lee, Y.S. Lim, N.C. Park, Y.C. Kim, Catalytic autothermal reforming of propane over the noble metal-doped hydrotalcite-type catalysts, Chem. Eng. J. 146 (2009) 295–301.
[35] F. Kovanda, E. Jindová, K. Lang, P. Kubát, Z. Sedláková, Preparation of layered double hydroxides intercalated with organic anions and their application in LDH/poly(butyl methacrylate) nanocomposites, Appl. Clay Sci. 48 (2010) 260–270.
[36] H.W. Olfs, L.O. Torres-Dorante, R. Eckelt, H. Kosslick, Comparison of different synthesis routes for Mg–Al layered double hydroxides (LDH): characterization of the structural phases and anion exchange properties, Appl. Clay Sci. 43 (2009) 459–464.
[37] J.I. Di Cosimo, V.K. Díez, M. Xu, E. Iglesia, C.R. Apesteguía, Structure and surface and catalytic properties of Mg–Al basic oxides, J. Catal. 178 (1998) 499–510.
[38] Y.C. Lin, Catalytic valorization of glycerol to hydrogen and syngas, Int. J. Hydrogen Energy 38 (2013) 2678–2700.
[39] C.A. Franchini, W. Aranzaez, A.M. Duarte de Farias, G. Pecchi, M.A. Fraga, Ce-substituted $LaNiO_3$ mixed oxides as catalyst precursors for glycerol steam reforming, Appl. Catal. B 147 (2014) 193–202.
[40] B. Katryniok, S. Paul, V. Bellière-Baca, P. Rey, F. Dumeignil, Glycerol dehydration to acrolein in the context of new uses of glycerol, Green Chem. 12 (2010) 2079–2098.
[41] H. Hattori, Solid base catalysis: fundamentals and applications, in: 20th Annual Saudi-Japan Symposium, Dhahran, Saudi Arabia, 2010.
[42] L.F. Bobadilla, A. Penkova, F. Romero-Sarria, M.A. Centeno, J.A. Odriozola, Influence of the acid–base properties over NiSn/MgO–Al_2O_3 catalysts in the hydrogen production from glycerol steam reforming, Int. J. Hydrogen Energy 39 (2014) 5704–5712.

[43] M.L. Dieuzeide, M. Jobbagy, N. Amadeo, Glycerol steam reforming over Ni/γ-Al_2O_3 catalysts, modified with Mg(II). Effect of Mg (II) content, Catal. Today 213 (2013) 50–57.
[44] L.F. Bobadilla, A. Álvarez, M.I. Domínguez, F. Romero-Sarria, M.A. Centeno, M. Montes, J.A. Odriozola, Influence of the shape of Ni catalysts in the glycerol steam reforming, Appl. Catal. B 123 (124) (2012) 379–390.
[45] M.L. Barbelli, F. Pompeo, G.F. Santori, N.N. Nichio, Pt catalyst supported on α-Al_2O_3 modified with CeO_2 and ZrO_2 for aqueous-phase-reforming of glycerol, Catal. Today 213 (2013) 58–64.
[46] A. Iriondo, V.L. Barrio, J.F. Cambra, P.L. Arias, M.B. Güemez, R.M. Navarro, M.C. Sanchez-Sanchez, J.L.G. Fierro, Influence of La_2O_3 modified support and Ni and Pt active phases on glycerol steam reforming to produce hydrogen, Catal. Commun. 10 (2009) 1275–1278.
[47] P. Ramirez de la Piscina, N. Homs, Use of biofuels to produce hydrogen (reformation processes), Chem. Soc. Rev. 37 (2008) 2459–2476.
[48] J.R. Rostrup-Nielsen, J. Sehested, J. Norskov, Hydrogen and synthesis gas by steam- and CO_2 reforming, Adv. Catal. 47 (2002) 65–139.
[49] D.L. Trimm, Coke formation and minimisation during steam reforming reactions, Catal. Today 37 (1997) 233–238.
[50] D.L. Trimm, Catalysts for the control of coking during steam reforming, Catal. Today 49 (1999) 3–10.
[51] A. Remiro, B. Valle, A.T. Aguayo, A.G. Gayubo, J. Bilbao, Operating conditions for attenuating Ni/La_2O_3-α-Al_2O_3 catalyst deactivation in the steam reforming of bio-pil aqueous fraction, Fuel Process. Technol. 115 (2013) 222–232.
[52] C. Wang, B. Dou, H. Chen, Y. Song, Y. Xu, X. Du, L. Zhang, T. Luo, C. Tan, Renewable hydrogen production from steam reforming of glycerol by Ni–Cu–Al, Ni–Cu–Mg, Ni–Mg catalysts, Int. J. Hydrogen Energy 38 (2013) 3562–3571.
[53] P. Kustrowśki, L. Chmielarz, E. Bożek, M. Sawalha, F. Roessner, Acidity and basicity of hydrotalcite derived mixed Mg–Al oxides studied by test reaction of MBOH conversion and temperature programmed desorption of NH_3 and CO_2, Mater. Res. Bull. 39 (2004) 263–281.
[54] L.F. Bobadilla, A. Penkova, A. Álvarez, M.I. Domínguez, F. Romero-Sarria, M.A. Centeno, J.A. Odriozola, Glycerol steam reforming on bimetallic NiSn/CeO_2–MgO–Al_2O_3 catalysts: influence of the support, reaction parameters and deactivation/regeneration processes, Appl. Catal. A 492 (2015) 38–47.
[55] L.M. Martínez, T.M. Araque, J.C. Vargas, A.C. Roger, Effect of Ce/Zr ratio in CeZr–CoRh catalysts on the hydrogen production by glycerol steam reforming, Appl. Catal. B 132–133 (2013) 499–510.
[56] M. El Doukkali, A. Iriondo, P.L. Arias, J.F. Cambra, I. Gandarias, V.L. Barrio, Bioethanol/glycerol mixture steam reforming over Pt and PtNi supported on lanthana or ceria doped alumina catalysts, Int. J. Hydrogen Energy 37 (2012) 8298–8309.